Journal of Materials Chemistry C

Accepted Manuscript

This article can be cited before page numbers have been issued, to do this please use: Y. Li, S. Bi, F. Liu, S. Wu, J. Hu, L. Wang, H. Liu and Y. Hu, *J. Mater. Chem. C*, 2015, DOI: 10.1039/C5TC00682A.

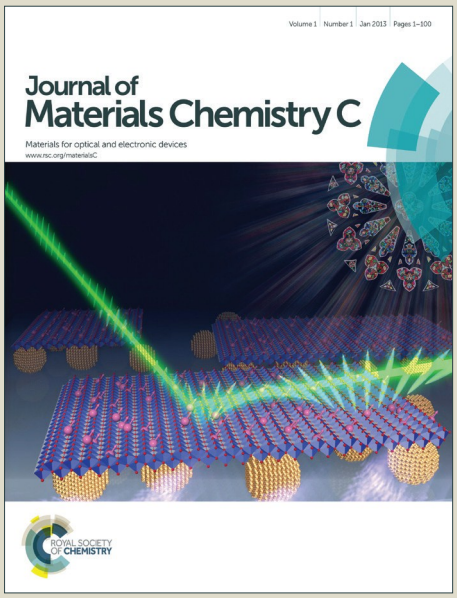

This is an *Accepted Manuscript*, which has been through the Royal Society of Chemistry peer review process and has been accepted for publication.

Accepted Manuscripts are published online shortly after acceptance, before technical editing, formatting and proof reading. Using this free service, authors can make their results available to the community, in citable form, before we publish the edited article. We will replace this *Accepted Manuscript* with the edited and formatted *Advance Article* as soon as it is available.

You can find more information about *Accepted Manuscripts* in the Information for Authors.

Please note that technical editing may introduce minor changes to the text and/or graphics, which may alter content. The journal's standard Terms & Conditions and the Ethical guidelines still apply. In no event shall the Royal Society of Chemistry be held responsible for any errors or omissions in this *Accepted Manuscript* or any consequences arising from the use of any information it contains.

ROYAL SOCIETY OF CHEMISTRY

www.rsc.org/materialsC

View Article Online
DOI: 10.1039/C5TC00682A

Journal Name

RSCPublishing

ARTICLE

Porosity induced emission: exploring color-controllable fluorescence of porous organic polymers and their chemical sensing applications†

Cite this: DOI: 10.1039/x0xx00000x

Received 00th January 2012,
Accepted 00th January 2012

DOI: 10.1039/x0xx00000x

www.rsc.org/

Yankai Li, ‡[a] Shiming Bi, ‡[b] Fei Liu,[a] Shengying Wu, [b] Jun Hu,*[a] Limin Wang,*[b] Honglai Liu[a] and Ying Hu[a]

Most organic dyes dissipate their excitation energy in the aggregated state because of "aggregation caused quenching" effect, deteriorating their application in optoelectronic devices. To prevent "aggregation caused quenching" effect, we incorporate a dye-based fluorophore into a porous organic polymer skeleton because porosity would breed the spatial isolation of fluorophores to maintain its emission. Tuning the fraction of fluorophores in the skeleton of FL-SNW-DPPs would range the emission color covering from red to blue in both solid-state and suspension. More importantly, the combination of fluorescence and porosity of FL-SNW-DPPs would provide more space to transduce the molecular interaction between adsorbed analytes and fluorophores to the detectable changes in light emission, leading to the fluorescence-off or fluorescence-on detection of electron-deficient or electron-rich analytes.

Introduction

Fluorescent materials has spurred flourishing research interests, for they lie at the crossroad of a wide range of applications, such as light-emitting motifs, fluorescent sensors, probes, and various luminescent displays[1-3]. Many fundamental researches of these materials, especially in the fields of analytical and biological chemistry, are conducted in solutions, due to their excellent selectivity, a wide linear range of analysis and convenience in handling[4-6]. Recently, the growing applications of new optoelectronic devices, like organic light-emitting diodes (OLEDs)[7] or fluorescent sensors[8], has motivated the development of materials displaying efficient fluorescence in the solid-state. However, most organic dyes, which exhibit excellent fluorescence in solutions or in suspensions, are non-luminescent in the solid state because the intimate contact among the molecules themselves result in "aggregation caused quenching" (ACQ)[4].

So far, two strategies are usually utilized to circumvent the ACQ challenge for dyes. One is known as the aggregation-induced emission[9]. For this approach, only a limited number of molecules, which share the common feature of freely rotatable peripheral aromatic arms, possess this property. The π-conjugation stack caused by the aggregation restricts the rotation of phenyl rings and results in the strong fluorescence. But in the solution, the free rotation of the molecules leads to quench the luminescence activity. Another is the steric hindrance effect, such as *via* the introduction of bulky-substituents, dendritic substituent protection[10], the fluorophores in the well-designed dye molecules can avoid the aggregation and hence keep the fluorescence. However, too complicated synthetic procedures restrict their applications. It still remains a great challenge to develop a facile way to fabricate the materials with fluorescence in the solid-state.

Recently, porous organic polymers (POPs), weaving small molecules into three-dimensional intrinsic networks have caused numerous attentions[11-16]. Several fluorescent POPs have been produced by either the in-situ polymerization or the post-modification methodologies[17]. For the in-situ polymerization, the fluorescence of POPs is contributed by large π-conjugation, and this kind of POPs are also known as conjugated microporous polymers (CMPs)[18-21]. The carefully designed monomers produce the extended π-conjugation in the crosslinking network *via* the coupling reactions, which generally require pricy monomers and expensive catalysts[22-24]. Recently, Jiang[25] et al. adopted a core-shell strategy to covalently link two CMPs with different fluorescence wavelength so that the color of the light emission were controlled by tuning the core/shell ratio or the core-shell structural order. Moreover, the special aggregation-induced emission molecules mentioned above also can be designed as monomers, through the polymerization, the peripheral phenyl groups were introduced and fixed into the network, which lead to POPs with strong fluorescence[26, 27]. For the post-modification, POPs with specific porosities have been obtained prior to the modification, and both physical loading[28] and chemical on-surface functionalization[29] can be used to obtain fluorescence POPs. Upon the delicate design, the guest-to-host energy transfer process would significantly improve the emission intensity of guest dye molecules, which is known as

ARTICLE View Article Online
DOI: 10.1039/C5TC00682A Journal Name

"light harvesting". Very recently, Guo[30] et al. combined the in-situ polymerization and the post-modification together to successfully produce a fluorescence POP. The POP namely NCMP with large conjugation was firstly synthesized; then, an organic dye of Nile Red was physically loaded into the pores of NCMP. Given that the adsorption band of Nile Red was exactly the emission band of NCMP, the fluorescence of Nile Red was enhanced through the energy transfer process between host and guest molecules. Because the structural characteristics and porosity of POPs can be easily tuned due to versatile building blocks and polymeric strategies, there still remains a wide scope in searching for distinct strategies to develop various fluorescence POPs.

Herein, we proposed a new strategy as "Porosity Induced Emission". By covalently incorporating dye-based monomers into the networks of POPs, the fluorophores can be spatially isolated by the porosity, thus it significantly enhances the fluorescence intensity of the monomers, which are originally suffered from the ACQ. A conventional copolymer strategy through a single-step and catalyst-free procedure was used to developed a novel fluorescence POP with the color-controllable emission. 4-diketopyrrolo[3,4-c]pyrrole (DPP), a commercial dye with the strong red light emission[31], was copolymerized into the skeleton of a melamine-based porous fluorescent network to form FL-SNW-DPPs with dual-light emission. Tuning the DPP fraction in the skeleton of FL-SNW-DPPs would range the emission covering from red to blue in both solid-state and suspension. More importantly, the combination of fluorescence and porosity would provide more space to transduce the molecular interaction between adsorbed analytes and fluorophores to the detectable changes in light emission[32], leading to the fluorescence-off or fluorescence-on detection of electron-deficient or electron-rich analytes.

Experimental Section

Materials and methods

Melamine, 4,4'-Biphenyldicarboxaldehyde was purchased from Sigma-Aldrich and TCI. Anhydrous DMSO and 2,4,6-trinitrophenylmethylnitramine standard solution were purchased from J&K Scientific Ltd., China. Nitrobenzene and picric acid were purchased from Sinopharm Chemical Reagent Co. Ltd., China. All other chemicals were purchased for alladin. All were used without any further purification. ^{1}H NMR spectra of small molecules were collected on a Bruker Avance DPS-300 spectrometer using $CDCl_3$ or DMSO-d_6 as solvent and tetra- methylsilane as an internal reference. Solid state ^{13}C cross-polarization (CP)/magic-angle spinning (MAS) NMR spectrum was recorded with a Varian Mercury-Plus 400 MHz spectrometer. Thermogravimetry analysis (TGA) were performed under N2 on a NETZSCH STA449F3, with a heating rate of 10 °C min^{-1}. Nitrogen adsorption isotherms were measured at 77 K using Micromeritics Tristar 3020 static volumetric analyzer. Before adsorption measurements the polymer was degassed at 150 °C under vacuum. The Brunauer-Emmett-Teller (BET) surface area was calculated within the relative pressure range 0.05 to 0.30. Total volume was calculated at p/p_0=0.98. The adsorption spectra were measured on a Shimadzu, UV-2550 spectrophotometer. UV-vis reflective spectra of solid sample were measured by Cary 500 UV-VIS Spectrophotometer. Fluorescence spectra were conducted on Hatachi F4500 fluorescence spectrophotometer at room temperature. Polymer samples were suspended in THF (2 mg/ 2 mL) to collect fluorescence data. Fluorescence quantum yield of FL-SNW-DPPs in THF was measured on a FluoroMax-4 fluorescence spectro-photometer by using an integrating sphere method. FT-IR data were obtained using a Nicolet Magna-IR 550 spectrometer. Elemental analysis was determined using a Vario EL III Elemental Analyzer (Elementar, Germany).

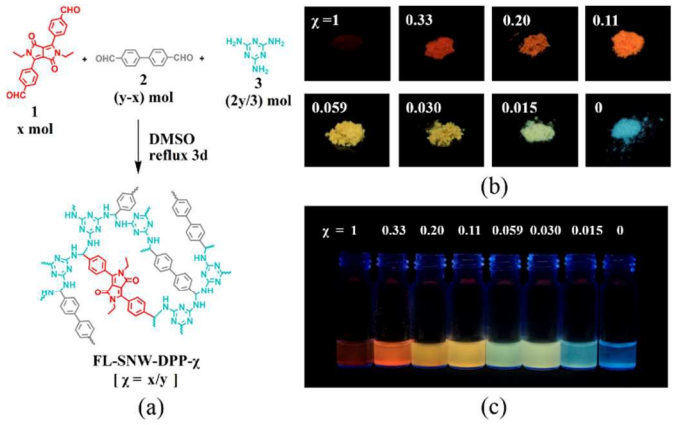

Fig. 1 (a) synthesis procedure of FL-SNW-DPPs; Photos of solid-state (b) and THF suspension (2 mg/2 mL) (c) of FL-SNW-DPPs under λ=365 nm using a UV lamp.

Calculations were performed at Density Function Theory (DFT) level with the hybrid functional B3LYP, which incorporates Becke's three-parameter exchange functional[33] and the Lee, Yang, and Parr correlation functional[34] using the Gaussian 09 program[35]. The 6-31G** basis sets[36] implemented in the Gaussian program were used. The geometries of ion pairs were fully optimized at the B3LYP/6-31G** level, and the basis set superposition error (BSSE)[37] was corrected for all interaction calculations using the counterpoise method[38, 39].

The synthetic procedure of monomer and the procedure of cycling test was described in ESI.

Synthesis procedure

By following a well-known method[40], a mixture of 4,4'-(2,5-diethyl-3,6-dioxo-2,3,5,6-tetrahydropyrrolo[3,4-c]pyrrole-1,4-diyl)dibenzaldehyde (1) with 4,4'-Biphenyldicarboxaldehyde (2)and melamine (3) was dissolved in DMSO and heated at 180 °C for 3 days to afford FL-SNW-DPP-χ. χ value is defined as the molar ratio of formyl group in 1 to the total ratio of formyl group originating from starting materials. The amounts of total formyl groups and amine groups in precursors were equal (Fig. 1a).

Typically, we take the synthesis of FL-SNW-DPP-0.11 as an example. An oven dried Schlenk flask fitted with a condenser and a magnetic stirring bar was charged with melamine (75 mg, 0.6 mmol), 4,4'-Biphenyldicarboxaldehyde (168 mg, 0.8 mmol), 4,4'-(2,5-diethyl-3,6-dioxo-2,3,5,6-tetrahydropyrrolo[3,4-c]pyrrole-1,4-diyl)dibenzaldehyde (40 mg, 0.1 mmol) and dimethyl sulfoxide (3.75 ml).After degassing by argon bubbling the mixture was heated to 180 °C for 72 h under an inert atomosphere. After cooling to room temperature the precipitated polymers was isolated by filtration over a Büchner funnel and washed with excess acetone, tetrahydrofurane and dichloromethane. Then the product was further extracted with acetone by Soxhlet apparatus for 24 h. The solvent was removed under vacuum at room temperature to afford the materials as orange powders (yield=54 %).

Journal Name

View Article Online
DOI: 10.1039/C5TC00682A

Results and discussion

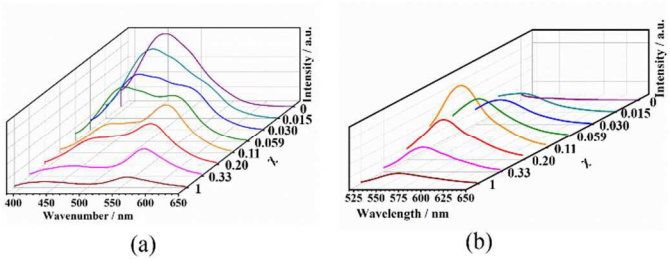

Fig. 2 Fluorescence spectrum for FL-SNW-DPP-χ in THF excited at 370 nm (a) and 500 nm (b).

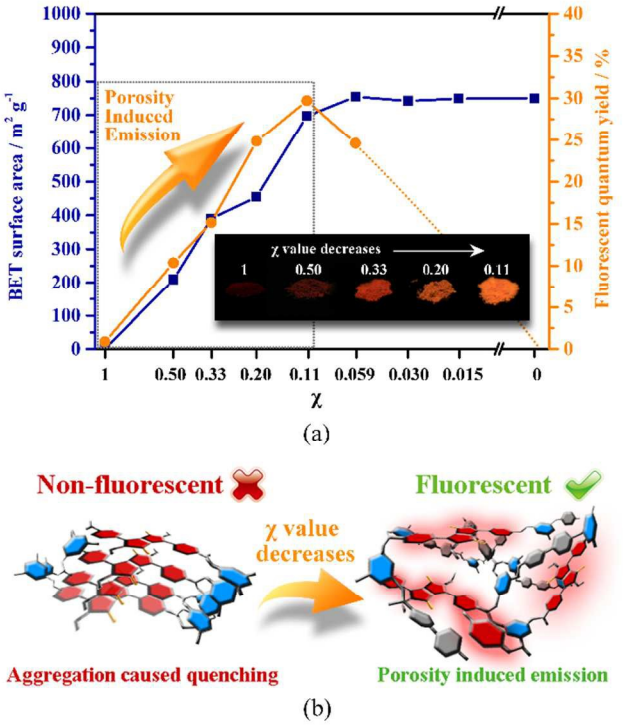

Fig. 3 (a) The trends of BET surface area and fluorescent quantum yield (Φ_{FL}) of DPP's emission as χ value decreases. Dash line represents predicted Φ_{FL} trend, where both the emission and adsorption of DPP moiety are very weak so that the result was obtained with great inaccuracy error. When the χ value is greater than 0.11 (inside the grey box), the trend of BET surface area and Φ_{FL} are similar, which is the proof of "porosity induced emission" effect. The posterior decline of Φ_{FL} trend mainly attributed to the reduction of DPP content in the skeleton. Inset: photos of FL-SNW-DPPs powders under λ=365 nm; (b) Representation of the mechanism of "porosity induced emission".

FL-SNW-DPPs were obtained as fine powders. As the χ value increased, the hue of the powders gradually turn from white to yellow then to red. Upon excited under the UV light, all FL-SNW-DPPs exhibit fluorescence in both solid-state and suspension, and the color of fluorescence range from red to blue (Fig. 1b-c). These powders are insoluble in common solvents including water, acetone, dimethylcholride, tetrahydrofuran, hexane, and dimethyl sulfoxide. Meanwhile, the color of FL-SNW-DPPs powders do not fade after refluxing in solvents, indicating the excellent stability due to the covalent incorporation of DPP. Thermogravimetric analysis proved that all FL-SNW-DPPs also exhibited high thermo-stability (T_{deg} > 350 °C) (Fig. S1, ESI).

Fourier transform infrared (FTIR) spectroscopy was conducted to confirm the structure of polymer (Fig. S2, ESI), the band near 1205 cm^{-1} and the absence of bands near 1600 cm^{-1} show the monomers are linked *via* C-N bond instead of C=N bond, which is similar to the previous literature[40]. The band near 1700 cm^{-1}, which is attributed to the amide structure in DPP moieties, enhances dramatically as the χ value increases, indicating the successful incorporation of DPP moieties into the network. Furthermore, the growing intensity of the adsorption band at 500 nm in UV-vis reflective spectra as the increase of χ value also serves as a strong evidence for the existence of DPP moieties in FL-SNW-DPPs (Fig S3, ESI). Solid state ^{13}C cross-polarization (CP)/magic-angle spinning (MAS) NMR spectra further confirm the molecular structure of networks (Fig. S4, ESI). To quantitatively measure the DPP content in the skeleton, N/C mass ratio of each FL-SNW-DPPs, determined by the elemental analysis, was calculated to illustrate the DPP density. After the calibration, the calculated DPP density is in accordance with the χ value. (Table S1-S2, Fig. S5, ESI).

Fluorescence spectra of FL-SNW-DPPs at room temperature were conducted to explore their light-emitting properties (Fig. 2 and Fig. S6, ESI). FL-SNW-DPPs exhibit dual emission bands at 467 nm and 550 nm (Fig. 2a), which are attributed to the emissions of SNW (Schiff-base network) and DPP moieties, respectively. The intensity of emission bands at 467 nm gradually dips as the χ value increases. The versatile color of light emission is actually engendered by the various intensities of both emissions. It is worth noting that the intensity of emission at 550 nm increases gently as the χ value increased and reaches a maximum when χ=0.11 (Fig. 2b). After that, the intensity anomalously decreases, rather than increases in accordance with the χ value. FL-SNW-DPP-1, which was supposed to exhibit the strongest red emission, in fact, emits very weak fluorescence.

To gain insight into the mechanism of this anomalous fluorescent intensity trend, a comparative analysis of the fluorescent quantum yield (Φ_{FL}) and the porosity was made (Fig. 3a). The N_2 adsorption isotherms at 77 K (Fig. S7, ESI) indicate the quite different porosities of FL-SNW-DPPs. FL-SNW-DPP-1 was characterized to be non-porous, attributed to the interpenetration caused by the strong stacks between the flat DPP moieties *via* the Van der Waals interaction during the polymerization[41, 42]. In this case, the DPP moieties are intimately contacted with each other, suffering from ACQ effects, hence the extremely weak emission and the lowest Φ_{FL} value of DPP moieties (0.58%). As the χ value decreases, the Brunauer-Emmett-Teller surface area value (S_{BET}) of FL-SNW-DPPs climbs dramatically, demonstrating that the stacking interactions between DPP moieties are gradually disrupted. The regularity of this proportionally increasing trend between the values of Φ_{FL} and S_{BET} as the χ value decreases from 1 to 0.11 demonstrates that improvement of the porosity leads to the spatial isolation of DPP dyes, which gradually liberates the luminescence from the ACQ effect (Fig. 3b). When the χ value is below a relatively low point (χ<0.11), the small amount of DPP moieties has less effect on the porosity and S_{BET} value almost remains as high as about 750 $m^2 g^{-1}$. Accordingly, DPP moieties are highly dispersed in the network. In this scope, the values of Φ_{FL} drops with the decreasing χ, indicating that the density of DPP moieties in the skeleton plays an important role to their emission. Therefore, both the porosity and the density of DPP moieties in the skeleton are two indispensable factors

View Article Online
DOI: 10.1039/C5TC00682A
Journal Name

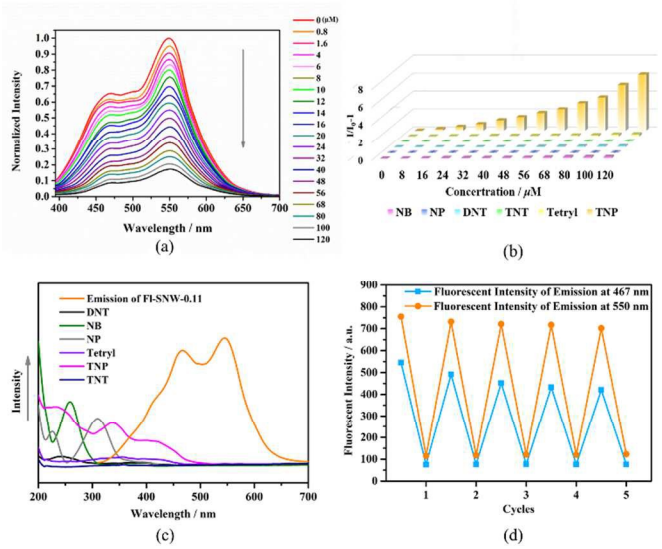

Fig. 4 (a) Effect on the emission spectra of THF suspension of FL-SNW-DPP-0.11 upon incremental addition of a TNP solution; (b) SV plots for the emissions at 467 nm of FL-SNW-DPP-0.11 upon addition of various nitro aromatics solution. (c) Spectral overlap between the absorption band of analytes and the emission spectrum of FL-SNW-DPP-0.11 in THF. (d) Cycling tests of FL-SNW-DPP-0.11 upon the addition of TNP (120 μM). The figure illustrates the fluorescent intensity plots of emission at both 467 nm (blue squares) and 550 nm (orange circles).

for the emission. These two factors reach to a compromise when χ=0.11, where Φ_{FL} value of DPP's emission (29.70%) reaches the highest. As we know, the fluorescence of dye in solution is attributed to the high dispersal of dyes in solvent, which is also known as the "cage effect". Similarly, for FL-SNW-DPPs, it is the porosity that breeds the spatial isolation of dye moieties, which efficiently detour the ACQ effect. Accordingly, we proposed this phenomenon as the "porosity induced emission". It should be noted that this "porosity induced emission" mechanism is quite different from the available intrinsic fluorescence POPs produced by the coupling reactions, since they are mechanically irrelative to their porosity.

The excellent porosity of FL-SNW-DPPs also ensures the accommodation of small molecules, which could be a specific sensor when the adsorbed molecules have strong interaction with the fluorophores. In this case, nitro aromatics including nitrobenzene (NB), 4-nitrophenol (NP), 2,4-dinitrotoluene (DNT), 2,4,6-trinitrotoluene (TNT), 2,4,6-trinitrophenyl-methylnitramine (Tetryl), and 2,4,6-trinitrotoluene (TNP) were selected as the analytes for chemical sensing study, among which, the most toxic and destructive compound of TNP was particularly concerned[43-45]. By an incremental addition of TNP into THF suspension of FL-SNW-DPP-0.11, the emission intensity at both 467 nm and 550 nm vanish rapidly (Fig. 4a), even can be detectable at very low TNP concentration (0.4 μM) (Fig. S8, ESI). While for the other nitro aromatics, little quenching efficiency was observed, indicating that FL-SNW-DPP-0.11 exhibited an excellent selectivity for TNP to other nitro aromatics. To quantify the quenching efficiency for various analytes, Stern-Volmer equation of $(I_0/I)=K_{sv}[A]+1$ was used, where I_0 and I represent the fluorescent intensity without and with the addition of analytes, [A] is the concentration of analyte and K_{sv} is the Stern-Volmer constant. The K_{sv} values are 5.3×10^4 M^{-1} and 4.1×10^4 M^{-1} upon the addition of TNP for the emission of 467 nm and 550 nm, respectively, which is much larger than those of other nitro aromatics (Fig. 4b and Fig. S9-S10, ESI).

The HOMO and LUMO energies of FL-SNW-DPPs and analytes were calculated to illuminate the mechanism of fluorescence quenching by nitro aromatics (Fig. S11-S12 and Table S3, details in ESI,). The LUMO of FL-SNW-DPP-0.11 lies at higher energy level than that of nitro aromatics, boosting a driving force of electron transfer from FL-SNW-DPP-0.11 to electron-deficient nitro aromatics, hence the quenching fluorescence. Besides, the SV plots of TNP for emissions at both 467 nm and 550 nm deviates upward from linearity at high concentration, while those of other nitro aromatics are linear. The nonlinear nature of the SV plots of TNP could be an evidence of the energy transfer process[43, 46]. Moreover, the emission spectra of FL-SNW-DPP-0.11 and nitro aromatics (Fig. 4c) show there is a greater spectral overlap between FL-SNW-DPP-0.11 and TNP. The spectral overlap further demonstrates the probability of energy transfer, thus amplifying the quenching efficiency.

In addition to the fluorescence-off detection of electron-deficient analytes, the fluorescent intensity of FL-SNW-DPP-0.11 can be enhanced upon the addition of electro-rich molecules like mesitylene (Fig. S13, ESI). On the contrary to the fluorescence-off phenomena, the higher LUMO energy of mesitylene shows a reversed driving force for the electron transfer, i.e. from the mesitylene to FL-SNW-DPP-0.11 (Fig. S14 and Table S4, ESI). Therefore, the fluorescence are enhanced. As a result, FL-SNW-DPP-0.11 can exhibit potency in both fluorescence-off and fluorescence-on dual-detections for electron-deficient and electron-rich analytes, respectively.

Furthermore, cycling tests were conducted to examine the stability of FL-SNW-DPP-0.11 as a chemical sensor (see details in ESI). Upon the addition of TNP (120 μM) to the THF suspension of FL-SNW-DPP-0.11, almost same quenching effect was observed for each cycle at both emissions of 467 nm and 550 nm (Fig. 4d). After successive washed with hot THF to remove the guest molecules, the regenerated FL-SNW-DPP-0.11 exhibit recovered fluorescent intensity. Little degradation of response time and sensitivity of FL-SNW-DPP-0.11 was observed after regeneration. Similarly, upon addition of mesitylene (5 mM), FL-SNW-DPP-0.11 showed the approximate enhancement in fluorescence after each cycle, and the fluorescent intensity drop to the original level after regeneration (Fig S15, ESI). Because of the insoluble nature of FL-SNW-DPP-0.11, it can be easily isolated with guest molecule. More importantly, much better than those fluorescence POPs produced by the physical loading modification, the regeneration would not deteriorate the sensing ability due to the excellent stability of FL-SNW-DPP-0.11 networks.

Conclusions

We presented a new strategy of "Porosity Induced Emission" for facilitating the synthesis of fluorescent POPs to detour the ACQ effect. The following are the conclusions. (1) The commercial dye DPP, which is non-emissive in the solid state, was covalently incorporated into the skeleton of FL-SNW-DPPs. The porosity breeds the spatial isolation of the DPP fluorophores, thus leads to the solid-state fluorescence. (2) The phenomenon that as the DPP density increased, the fluorescence intensity of DPP increased to a maximum but then dropped, was illustrated through a comparative analysis of the

Journal Name

View Article Online
DOI: 10.1039/C5TC00682A ARTICLE

fluorescent quantum yield (Φ_{FL}) and the BET surface area of a series of FL-SNW-DPPs, which revealed the mechanism of "Porosity Induced Emission". (3) Tuning the density of DPP moieties in the network could control the color of fluorescence of FL-SNW-DPPs, covering a broad range of color from red to blue. (4) FL-SNW-DPP-0.11 showed a selective fluorescence-off response to TNP quenching and a fluorescence-on response to mesitylene. Therefore, the "Porosity Induced Emission" approach can be an effective way to design materials with the solid-state fluorescence. This approach would be extensively applied for the common dye molecules to be emissive in the solid-state, which would be further applied as chemical sensors.

Acknowledgements

The work was supported by the National Basic Research Program of China (2013CB733501), the National Nature Science Foundation of China (No. 91334203, 21376074, 21272069, 20672035), the 111 Project of China (No.B08021) the Fundamental Research Funds for the Central Universities, the project of FP7-PEOPLE-2013-IRSES (PIRSES-GA-2013-612230) and the Key Laboratory of Organofluorine Chemistry, Shanghai Institute of Organic Chemistry, Chinese Academy of Sciences.

Notes and references

[a] *State Key Laboratory of Chemical Engineering and Department of Chemistry, East China University of Science and Technology, Shanghai, 200237, China.*
E-mail: junhu@ecust.edu.cn; Fax: +86 021 6425 2195; Tel: +86 21 6425 2195
[b] *Key Laboratory for Advanced materials and Department of Chemistry, East China University of Science and Technology, Shanghai, 200237, China.*
E-mail: wanglimin@ecust.edu.cn; Fax: +86 021 6425 3881 ; Tel: +86 21 6425 3881
‡ These authors contributed equally to this work and should be considered co-first authors.
† Electronic supplementary information (ESI) available: For details of experimental sections, physical properties and chemical sensing applications of FL-SNW-DPPs. See DOI:

1 S. Varughese, *Journal of Materials Chemistry C*, 2014, **2**, 3499.
2 K. Benelhadj, J. Massue, P. Retailleau, S. Chibani, B. Le Guennic, D. Jacquemin, R. Ziessel and G. Ulrich, *Eur. J. Org. Chem.*, 2014, **32**, 7156.
3 S. P. Anthony, *ChemPlusChem*, 2012, **77**, 518.
4 S. W. Thomas, G. D. Joly and T. M. Swager, *Chem. Rev.*, 2007, **107**, 1339.
5 T. E. Kaiser, H. Wang, V. Stepanenko and F. Würthner, *Angew. Chem. Int. Ed.*, 2007, **46**, 5541.
6 A. Wakamiya, K. Mori and S. Yamaguchi, *Angew. Chem. Int. Ed.*, 2007, **46**, 4273.
7 W.-Y. Wong and C.-L. Ho, *J. Mater. Chem.*, 2009, **19**, 4457.
8 H. N. Kim, Z. Guo, W. Zhu, J. Yoon and H. Tian, *Chem. Soc. Rev.*, 2011, **40**, 79.
9 R. Hu, N. L. C. Leung and B. Z. Tang, *Chem. Soc. Rev.*, 2014, **43**, 4494.
10 T. Sato, D.-L. Jiang and T. Aida, *J. Am. Chem. Soc.*, 1999, **121**, 10658.
11 R. Dawson, A. I. Cooper and D. J. Adams, *Prog. Polym. Sci.*, 2012, **37**, 530.
12 Z. Xiang and D. Cao, *Journal of Materials Chemistry A*, 2013, **1**, 2691.
13 Y. Xu, S. Jin, H. Xu, A. Nagai and D. Jiang, *Chem. Soc. Rev.*, 2013, **42**, 8012.
14 D. Wu, F. Xu, B. Sun, R. Fu, H. He and K. Matyjaszewski, *Chem. Rev.*, 2012, **112**, 3959.
15 J. W. Colson and W. R. Dichtel, *Nat Chem*, 2013, **5**, 453.
16 Z. Chang, D.-S. Zhang, Q. Chen and X.-H. Bu, *PCCP*, 2013, **15**, 5430.
17 A. Patra and U. Scherf, *Chemistry – A European Journal*, 2012, **18**, 10074.
18 J. Weber and A. Thomas, *J. Am. Chem. Soc.*, 2008, **130**, 6334.
19 Z. Xiang and D. Cao, *Macromol. Rapid Commun.*, 2012, **33**, 1184.
20 X. Liu, Y. Xu and D. Jiang, *J. Am. Chem. Soc.*, 2012, **134**, 8738.
21 L. Chen, Y. Honsho, S. Seki and D. Jiang, *J. Am. Chem. Soc.*, 2010, **132**, 6742.
22 Y. Xu and D. Jiang, *Chem. Commun.*, 2014, **50**, 2781.
23 J. Brandt, J. Schmidt, A. Thomas, J. D. Epping and J. Weber, *Polymer Chemistry*, 2011, **2**, 1950.
24 J. Schmidt, M. Werner and A. Thomas, *Macromolecules*, 2009, **42**, 4426.
25 Y. Xu, A. Nagai and D. Jiang, *Chem. Commun.*, 2013, **49**, 1591.
26 Q. Chen, J.-X. Wang, F. Yang, D. Zhou, N. Bian, X.-J. Zhang, C.-G. Yan and B.-H. Han, *J. Mater. Chem.*, 2011, **21**, 13554.
27 Y. Xu, L. Chen, Z. Guo, A. Nagai and D. Jiang, *J. Am. Chem. Soc.*, 2011, **133**, 17622.
28 L. Chen, Y. Honsho, S. Seki and D. Jiang, *J. Am. Chem. Soc.*, 2010, **132**, 6742.
29 H. Lim and J. Y. Chang, *Macromolecules*, 2010, **43**, 6943.
30 P. Zhang, K. Wu, J. Guo and C. Wang, *ACS Macro Lett.*, 2014, **3**, 1139.
31 M. Kaur and D. H. Choi, *Chem. Soc. Rev.*, 2015, **44**, 58.
32 A. Lan, K. Li, H. Wu, D. H. Olson, T. J. Emge, W. Ki, M. Hong and J. Li, *Angew. Chem. Int. Ed.*, 2009, **48**, 2334.
33 A. D. Becke, *The Journal of Chemical Physics*, 1993, **98**, 5648.
34 C. Lee, W. Yang and R. Parr, *Phys. Rev. A*, 1988, **38**, 3098.
35 G. W. T. M.J. Frisch, H.B. Schlegel, G.E. Scuseria, M.A. Robb, J.R. Cheeseman, G. Scalmani, V. Barone, B. Mennucci, G.A. Petersson, H. Nakatsuji, M. Caricato, X. Li, H.P. Hratchian, A.F. Izmaylov, J. Bloino, G. Zheng, J.L. Sonnenberg, M. Hada, M. Ehara, K. Toyota, R. Fukuda, J. Hasegawa, M. Ishida, T. Nakajima, Y. Honda, O. Kitao, H. Nakai, T. Vreven, J.A. Montgomery, Jr., J.E. Peralta, F. Ogliaro, M. Bearpark, J.J. Heyd, E. Brothers, K.N. Kudin, V.N. Staroverov, R. Kobayashi, J. Normand, K. Raghavachari, A. Rendell, J.C. Burant, S.S. Iyengar, J. Tomasi, M. Cossi, N. Rega, J.M. Millam, M. Klene, J.E. Knox, J.B. Cross, V. Bakken, C. Adamo, J. Jaramillo, R. Gomperts, R.E. Stratmann, O. Yazyev, A.J. Austin, R. Cammi, C. Pomelli, J.W. Ochterski, R.L. Martin, K. Morokuma, V.G. Zakrzewski, G.A. Voth, P. Salvador, J.J. Dannenberg, S. Dapprich, A.D. Daniels,. Farkas, J.B. Foresman, J.V. Ortiz, J. Cioslowski, D.J. Fox, Gaussian 09, Gaussian Inc., Wallingford, CT, 2009.
36 M. J. Frisch, J. A. Pople and J. S. Binkley, *The Journal of Chemical Physics*, 1984, **80**, 3265.
37 H. B. Jansen and P. Ros, *Chem. Phys. Lett.*, 1969, **3**, 140.

View Article Online
DOI: 10.1039/C5TC00682A
Journal Name

38 S. F. Boys and F. Bernardi, *Mol. Phys.*, 1970, **19**, 553.
39 M. M. Szczęśniak and S. Scheiner, *The Journal of Chemical Physics*, 1986, **84**, 6328.
40 M. G. Schwab, B. Fassbender, H. W. Spiess, A. Thomas, X. Feng and K. Müllen, *J. Am. Chem. Soc.*, 2009, **131**, 7216.
41 Z. Hao and A. Iqbal, *Chem. Soc. Rev.*, 1997, **26**, 203.
42 C. M. Thompson, F. Li and R. A. Smaldone, *Chem. Commun.*, 2014, **50**, 6171.
43 S. S. Nagarkar, B. Joarder, A. K. Chaudhari, S. Mukherjee and S. K. Ghosh, *Angew. Chem.*, 2013, **125**, 2953.
44 W. Zhang, L.-G. Qiu, Y.-P. Yuan, A.-J. Xie, Y.-H. Shen and J.-F. Zhu, *J. Hazard. Mater.*, 2012, **221–222**, 147.
45 S. S. Nagarkar, A. V. Desai and S. K. Ghosh, *Chem. Commun.*, 2014, **50**, 8915.
46 W. Wu, S. Ye, G. Yu, Y. Liu, J. Qin and Z. Li, *Macromol. Rapid Commun.*, 2012, **33**, 164.

View Article Online
DOI: 10.1039/C5TC00682A

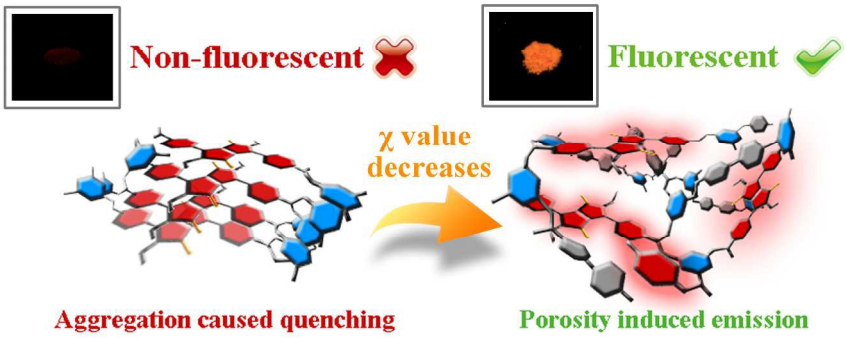

The strategy "Porosity Induced Emission" was presented for the synthesis of POPs with tunable fluorescence color and chemical sensing applications.
344x160mm (300 x 300 DPI)